Temperature Dependence of Homogeneous Nucleation in Ice

Haiyang Niu,[1,2,*] Yi Isaac Yang,[1,2] and Michele Parrinello[1,2,3,†]
[1]Department of Chemistry and Applied Biosciences, ETH Zurich c/o USI Campus, Via Giuseppe Buffi 13, 6900 Lugano, Switzerland
[2]Facoltà di Informatica, Instituto di Scienze Computationali, and National Center for Computational Design and Discovery of Novel Materials MARVEL, Università della Svizzera Italiana, Via Giuseppe Buffi 13, 6900 Lugano, Switzerland
[3]Istituto Italiano di Tecnologia, Via Morego 30, 16163 Genova, Italy

(Received 30 January 2019; revised manuscript received 6 May 2019; published 21 June 2019)

Ice nucleation is a process of great relevance in physics, chemistry, technology, and environmental sciences; much theoretical effort has been devoted to its understanding, but it still remains a topic of intense research. We shed light on this phenomenon by performing atomistic based simulations. Using metadynamics and a carefully designed set of collective variables, reversible transitions between water and ice are able to be simulated. We find that water freezes into a stacking disordered structure with the all-atom transferable intermolecular potential with 4 points/ice (TIP4P/ice) model, and the features of the critical nucleus of nucleation at the microscopic level are revealed. We have also estimated the ice nucleation rates along with other nucleation parameters at different undercoolings. Our results are in agreement with recent experimental and other theoretical works, and they confirm that nucleation is preceded by a large increase in tetrahedrally coordinated water molecules.

DOI: 10.1103/PhysRevLett.122.245501

Ice nucleation from water is a ubiquitous phenomenon [1] that is relevant in many areas of science and technology, from atmospheric and environmental science to aviation technology and biology. Understanding this process microscopically is of great value [2–4]. Interest in homogeneous ice nucleation in undercooled water also stems from the fact that it occurs in the so-called no man's land temperature region. Thus, it offers a tool to investigate the behavior of water in this part of the phase diagram that is deemed to be important for the understanding of water anomalies. Unfortunately, a direct simulation of this phenomenon is not possible, given the timescale over which crystallization takes place. This has made it difficult to reproduce the pioneering work of Ohmine and co-workers [5], in which one spontaneous nucleation event was reported. For this reason, a number of simulations with different methods (i.e., seeding approaches [6–10], enhanced sampling methods [9,11–16], or forward-flux sampling [17–19]) have been carried out. However, reversible transitions between ice and water and direct nucleation simulations of ice remain a great challenge, especially when using an all-atom water potential.

In this Letter, we carry out metadynamics (METAD) [20–22] by also combining it with integrated tempering sampling (METAITS) [23] simulations to investigate ice nucleation. As is common with other enhanced sampling methods [24,25], METAD requires the introduction of appropriate collective variables (CVs). If the CVs are properly chosen (that is, if they reflect the physics underlying the process), convergence is smooth. In a different context, we have shown that the x-ray diffraction peak intensities are useful CVs in the study of crystallization. For instance, they have been successfully applied to a system as complex as silica [26]. In some ways, silica has a behavior not too dissimilar from water. For instance, it exhibits a density anomaly [27]. Thus, it felt natural to continue using the same class of CVs.

Here, we propose two collective variables: one is a suitable combination of scattering peak intensities and has a long range character, and the other is a surrogate for translational entropy that has a more local nature. Importantly, these collective variables do not prejudge the ice structure to be formed. Using the all-atom transferable intermolecular potential with 4 points/ice (TIP4P/ice) model [28], we found that water freezes into a stacking disordered structure. We also calculated the temperature dependence of the nucleation behavior and the nucleation rates at different undercoolings. We can follow in detail the nucleation process, and the features of the critical nucleation nucleus have been discussed.

Even though hexagonal ice (ice I_h) is the stable crystal phase at ambient pressure, stacking-disordered ice (ice I_{sd}) consisting of random sequences of cubic and hexagonal ice layers is commonly observed in both experiments and simulations [9,15,19,29–31]. We chose a CV that is blind with respect to the form of ice polytypes that can be formed: I_h, I_{sd}, or cubic ice I_c. To this effect, one of the CVs is constructed as a linear combination of seven descriptors [32] (see the Supplemental Material [32] and Fig. S1 for how we chose these descriptors):

$$s_X = s_{100} + s_{002} + s_{101} + \alpha(s^{xy}_{100} + s^{xy}_{\bar{1}20}) + \beta s^{xz}_{002} + \gamma x^{yz}_{002}, \tag{1}$$

in which the first three descriptors correspond to the x-ray diffraction intensities of the three main peaks of the system, and s^{xy}_{100} and s^{xy}_{120} correspond to the intensities of the two main peaks of one single honeycomb bilayer, which is projected into the x-y plane; the last two descriptors of s^{xz}_{002} and s^{yz}_{002} refer to the intensity of the first main peak of the layers that are vertical to the honeycomb bilayer in the x-z and y-z planes, respectively. The coefficients α, β, and γ adjust the weights between different descriptors that are, in this work, $\alpha = 2$, $\beta = 1$, and $\gamma = 1$. This particular combination has proven to be efficient in accelerating nucleation.

In addition, we found it useful to combine the long-range order CV s_X with another CV that has a more local character: that is, the surrogate for translational entropy s_S, which has been successfully used elsewhere [37,38]. This additional CV proved important in accelerating the simulation convergence. The simulations that use s_X and s_S converge much faster than those using only s_X, in spite of the higher dimensionality of the CV space (see Fig. S2) [32]. This could be ascribed to the fact that s_S accelerates the melting of ice and, during crystallization, helps clearing defects. On the other hand, long-range order based CVs are essential in simulating ice nucleation because s_S alone cannot lead to nucleation.

Full technical details can be found in the Supplemental Material [32]. We only note here that the sampling efficiency is very high in standard METAD and even higher in METAITS, where the properties of the system in a whole range of temperatures can be calculated at a cost comparable to a single METAD run [23]. We have used the TIP4P/ice model of water [28], which has been explicitly designed to describe the solid phases of water. The melting temperature of the TIP4P/ice model is 270 K according to the most recent estimate [39]. The pressure has been set to its atmospheric value using a Parrinello-Rahman barostat [40] that allows only orthorhombic fluctuations.

We first performed the METAD simulation at 230 K. In Figs. S2 and S3 [32], we see how the two order parameters allow us to go reversibly from liquid to a stacking-disordered ice I_{sd}, which is consistent with experimental and other theoretical works [9,15,19,29,30]. The high sampling efficiency and the reversible transitions allow us to draw, in Fig. 1(a), the free energy surface (FES) as a function of the chosen CVs. As expected, at this temperature, the solid phase minimum is much lower than the liquid one. On this surface, an almost linear free energy path can be tracked that goes from liquid to solid. The barrier to this transition is $\triangle G = 52.8 \pm 6\ k_B T$, which is in agreement with other theoretical predications based on classical nucleation theory [19]. To quantify the characteristic of the stacking-disordered ice I_{sd} that was obtained from nucleation, we have calculated the cubicity (i.e., the fraction of cubic stacking sequences) of the obtained solids for over 60 nucleation events; the results show that the probability follows a distribution with a mean cubicity

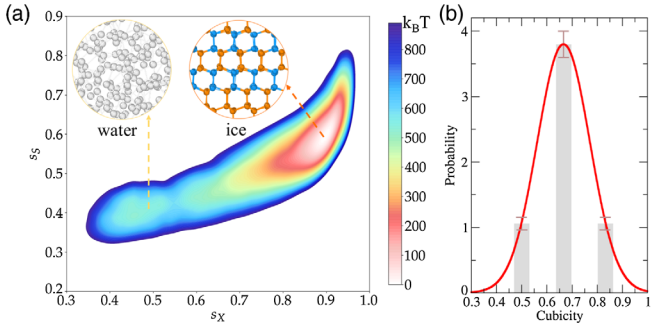

FIG. 1. Free energy surface in terms of collective variables s_X and s_S with TIP4P/ice model. (a) Free energy surface at 230 K for a system of 1600 water molecules. (b) Probability distribution of the cubicity of the nucleated ice structure obtained from simulations.

value of $C^* = 0.67 \pm 0.10$, as shown in Fig. 1(b), which is comparable to that ($C^* = 0.63 \pm 0.05$) obtained with the coarse-grained monotonic water (MW) potential [9]. Furthermore, the cubic and hexagonal sequences are randomly arranged, which result in a lower symmetry trigonal I_{sd} structure with the space group $P3m1$ (see Fig. S4) [32,41].

Having harvested a large number of crystallization events, we have enough statistics to address the issue of nucleation. In classical nucleation theory, which is the theoretical cornerstone in nucleation studies, the free energy as a function of the solidlike cluster size plays a pivotal role. For this reason, we first identify a variable that is able to distinguish between solidlike and liquidlike atoms. In the spirit of our work, we sit on each atom and calculate the instantaneous scattering intensity of that particular atom to the CV s_X (see Fig. S5) [32,42]. This fingerprint is able to distinguish between solidlike and liquidlike atoms well. Then, we identify all the solidlike atom clusters and make a histogram as a function of $n^{1/3}$, where n is the number of atoms in a solidlike cluster. The quantity $n^{1/3}$ is proportional to the cluster radius. In order to determine system size effects, we have performed calculations at 230 K for three different systems with $N = 896$, 1600, and 2880 water molecules, respectively. Figure 2(a) shows that the curve of $N = 1600$ is indistinguishable from that of $N = 2880$, whereas divergence can be noticed for that of $N = 896$ at relatively higher n. Thus, system size effects can be ruled out for system sizes larger than 1600 because, from this size on, the critical nucleus fits into the simulation box. Our estimate of the critical nucleus [see Fig. 2(b)] size gives a value of $N_c = 314 \pm 20$, which is in agreement with other theoretical estimates [19]. This number is temptingly close to $N_c = 321$, which is the number of water molecules contained in a microcrystallite, for which the shape is depicted in Fig. 2(c). This suggestion is strengthened by the fact that some faceting can be observed in a visual inspection. We must add that, in the morphology of the typical critical

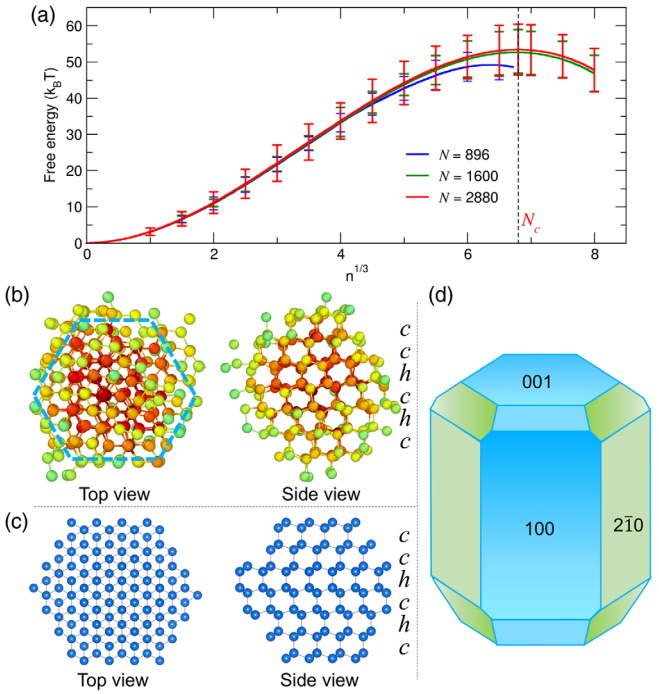

FIG. 2. Features of critical nucleus of ice nucleation. (a) Reweighted free energy at 230 K as a function of ice cluster size $n^{1/3}$ for a system with $N = 896$, 1600, and 2880 water molecules. (b)–(c) Typical critical ice nucleus and idealized crystalline model of it. Here, h and c refer to the hexagonal and cubic sequences of I_{sd}. (d) Possible crystal shape of I_{sd} with a threefold rotational symmetry.

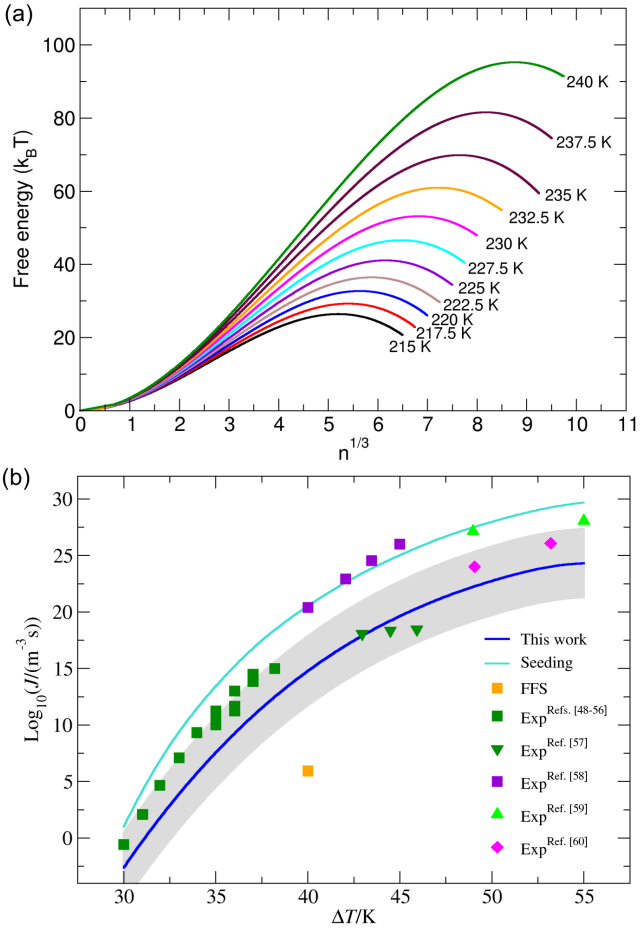

FIG. 3. Temperature dependence of ice nucleation behavior. (a) Reweighted free energy as a function of ice cluster size $n^{1/3}$ for a range of temperatures from 215 to 240 K. (b) Ice nucleation rate $\log_{10}J$ as a function of the supercooling temperature ΔT (difference between the melting temperature and the temperature of interest) obtained in this work and comparison with experimental [48–60] and other theoretical results [19,47]. Theoretical results denoted as FFS and seeding were estimated with forward-flux sampling [19] and a seeding technique [47], respectively.

nucleus, variations around this shape are seen. The microcrystallite in Fig. 2(c) could thus be thought of as an idealized representation of the critical nucleus shape. According to this picture, the critical nucleus is close to being spherical and appears to have a threefold rotational symmetry, in accordance with the space group ($P3m1$) of I_{sd}, which can be expected to grow into trigonal symmetry ice [Fig. 2(d)] [43]. Furthermore, when ice nuclei of sizes slightly larger than the critical one are evolved without bias, they tend to morph spontaneously into a shape resembling the one in Fig. 2(b) (see Fig. S6).

In order to independently check whether this nucleus belongs to the transition state ensemble, we have performed as many as 50 independent trajectories, starting from a water configuration that has been equilibrated in the presence of the ideal crystalline in Fig. 2(c). In the equilibration time, the atomic positions of the crystalline were held in place by a restraining potential. Once this potential was released, unbiased molecular dynamics simulations were performed. In 50 independent simulations, around 56 and 44% of the trajectories showed that the ice nuclei grew and melted, respectively, which indicates our estimation of the critical size is in the right ballpark. Furthermore, some trajectories showed that the ice nuclei neither grew nor melted in 500 ns simulations, which indicates that the potential energy surface around the critical ice cluster is rather flat, which is coherent with the transition state shape in Fig. 2.

By using METAITS, we have studied the temperature dependence of the nucleation energy barrier ΔG, the critical nucleus size N_c, and the nucleation rate J as shown in Fig. 3. The latter is computed by following the approach described in Refs. [44–46]. We checked that, at a selected number of temperatures (220, 225, 230, and 235 K), the standard METAD simulations gave the same results as METAITS (see Table SI [32]). This was indeed the case, as expected. Our estimate gives the nucleation rate $\log_{10}J$ (with J in units of the number of critical clusters per cubic meter per second) at 230 K as 14.8 ± 2.7, which lies in between the values of 5.93 (obtained in a forward-flux sampling calculation [19]) and 20.5 (with the seeding technique [47]). Our results can

also be compared with experimental values [48–60] that, in most cases, are slightly higher than our estimations. As the temperature is decreased, a continuous growth of the nucleation rate J is observed, which is in consistent with the experimental results [61] and the theoretical results obtained with the seeding technique [47].

Many theoretical and experimental works [62–70] have been devoted to understanding the mechanistic insight of the structural transformation from water to ice. With the coarse-grained MW potential, Molinero and co-workers [64,65] have uncovered that the rate of homogeneous nucleation of ice is controlled by the structural transformation into a four-coordinated liquid, and ice nucleates mostly within the four-coordinated liquid patches. In order to analyze the nucleation process with the all-atom TIP4P/ice model, we have plotted the configuration snapshots of one typical nucleation process at 230 K (Fig. 4), in which the tetrahedral-like and icelike atoms are tracked. We show here the results for the 230 K case, but similar results are observed at all the other temperatures. The tetrahedral-like atom is identified by the tetrahedral order parameter [71,72], in which both the distances and angles between the oxygen atoms are taken into account. Our results show that the patches of tetrahedrally coordinated water molecules play a central role because the precursor structure for ice nucleation and ice clusters nucleates from these patches, which is in agreement with experimental [62] and other theoretical works [63–65,69]. This can be seen in Fig. 4(d), in which, before the critical nucleus size is reached, the number of tetrahedral-like water $\Delta N_{\mathrm{tetra}}$ is much larger than those that have a local solidlike environment, which is in accordance with Moore and Molinero's observations with the coarse-grained MW potential [64]. A recent work by Fitzner *et al.* [66] reported that ice nuclei appear to originate from regions of low mobility; this is fully consistent with our observation because less mobile regions have a higher degree of tetrahedral order, as shown by Tanaka [63]. As the nucleation process advances, $\Delta N_{\mathrm{ice}} - \Delta N_{\mathrm{tetra}}$ becomes smaller until $\Delta N_{\mathrm{ice}} \approx \Delta\ N_{\mathrm{tetra}}$ in the proximity of the critical size. These results can also explain why the CV s_S with a local structure nature is essential to enhancing ice nucleation. In our simulations, we also observed that several ice clusters can be formed in the simulation box: in some cases, one cluster grows while others dissolve; in others, two or even more clusters can grow together until they merge into one cluster (see Fig. S9) [32]. The size of such a merged cluster could instantaneously surpass the size of the critical cluster.

In this Letter, our findings show that the formation of ice from undercooled water can be successfully simulated with the all-atom TIP4P/ice model by using the enhanced sampling methods METAD and METAITS. To induce this transition, we have proposed two collective variables. They are the intensities of properly selected scattering peaks that are more sensitive to long range order and a surrogate for translational entropy that gives local information.

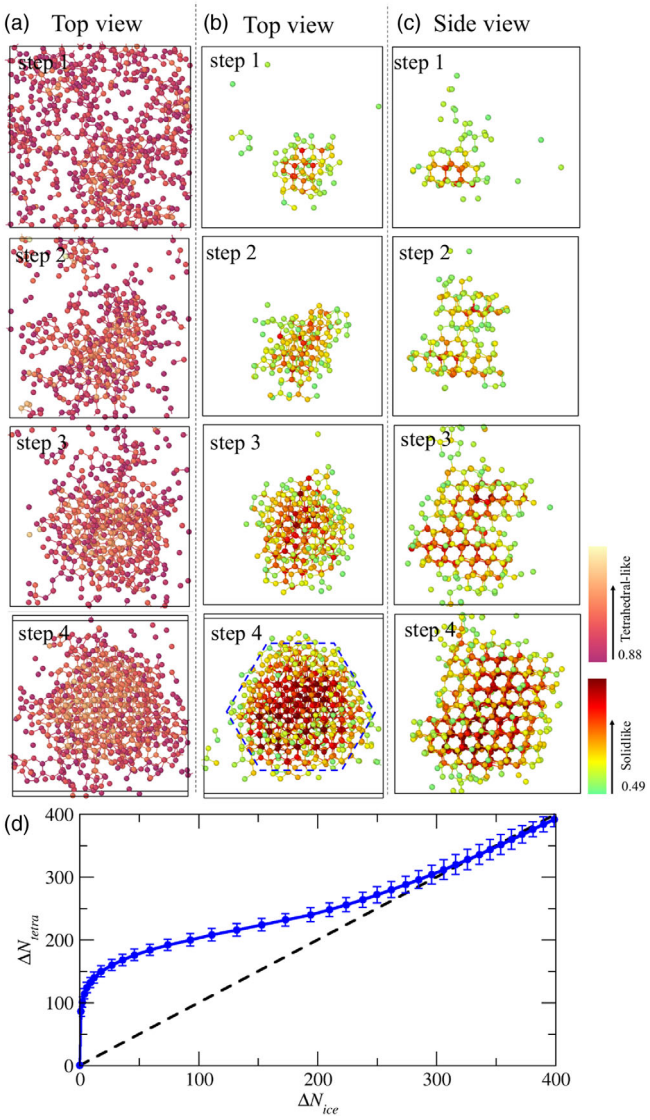

FIG. 4. Homogeneous ice nucleation process. Configuration snapshots at different stages of nucleation of (a) tetrahedral-like atoms and (b)–(c) solidlike atoms. (d) Relationship between the numbers of solidlike atoms ΔN_{ice} and tetrahedral-like atoms $\Delta N_{\mathrm{tetra}}$. Here, $\Delta N_{\mathrm{tetra}}$ is the difference between the tetrahedral-like atoms number of the current state and the tetrahedral-like atoms number of the liquid state.The dashed line is drawn only to guide the eyes.

Our results demonstrate that stacking-disordered ice can be formed directly from water at homogeneous conditions with a mean cubicity of $C* = 0.67 \pm 0.10$ and a critical size of $N_c = 314 \pm 20$ at 230 K. The barrier of ice nucleation at this temperature is estimated to be $\triangle G = 52.8 \pm 6\ k_B T$. We also find that ice nucleates from the tetrahedrally coordinated structure patches, in agreement with experimental and other theoretical works. Furthermore, the temperature dependence of the nucleation behavior is addressed, and the nucleation rates at different undercoolings are estimated. Our work makes studying the ice formation with all-atom water potential possible, and it

is a starting point for investigating more sophisticated ice nucleation problems, such as uncovering active sites in heterogeneous ice nucleation and the nature of antifreezing protein.

This research was supported by the NCCR MARVEL, funded by the Swiss National Science Foundation, and European Union Grant No. ERC-2014-AdG-670227/VARMET. The computational time for this work was provided by ETH Zurich and the Swiss National Supercomputing Center (CSCS) under Project mr22. The calculations were performed using the Piz Daint cluster at the CSCS and the Euler cluster at ETH Zurich.

*haiyang.niu@phys.chem.ethz.ch
†parrinello@phys.chem.ethz.ch

[1] T. Bartels-Rausch, V. Bergeron, J. H. E. Cartwright, R. Escribano, J. L. Finney, H. Grothe, P. J. Gutiérrez, J. Haapala, W. F. Kuhs, J. B. C. Pettersson *et al.*, Rev. Mod. Phys. **84**, 885 (2012).
[2] T. Bartels-Rausch, Nature (London) **494**, 27 (2013).
[3] I. Coluzza, J. Creamean, M. J. Rossi, H. Wex, P. A. Alpert, V. Bianco, Y. Boose, C. Dellago, L. Felgitsch, J. Fröhlich-Nowoisky *et al.*, Atmosphere-Ocean **8**, 138 (2017).
[4] A. Kiselev, F. Bachmann, P. Pedevilla, S. J. Cox, A. Michaelides, D. Gerthsen, and T. Leisner, Science **355**, 367 (2017).
[5] M. Matsumoto, S. Saito, and I. Ohmine, Nature (London) **416**, 409 (2002).
[6] E. Sanz, C. Vega, J. Espinosa, R. Caballero-Bernal, J. Abascal, and C. Valeriani, J. Am. Chem. Soc. **135**, 15008 (2013).
[7] J. R. Espinosa, A. Zaragoza, P. Rosales-Pelaez, C. Navarro, C. Valeriani, C. Vega, and E. Sanz, Phys. Rev. Lett. **117**, 135702 (2016).
[8] J. R. Espinosa, C. Vega, C. Valeriani, and E. Sanz, J. Chem. Phys. **144**, 034501 (2016).
[9] L. Lupi, A. Hudait, B. Peters, M. Grünwald, R. G. Mullen, A. H. Nguyen, and V. Molinero, Nature (London) **551**, 218 (2017).
[10] B. Cheng, C. Dellago, and M. Ceriotti, Phys. Chem. Chem. Phys. **20**, 28732 (2018).
[11] D. Quigley and P. Rodger, J. Chem. Phys. **128**, 154518 (2008).
[12] A. Reinhardt and J. P. Doye, J. Chem. Phys. **136**, 054501 (2012).
[13] A. Reinhardt, J. P. Doye, E. G. Noya, and C. Vega, J. Chem. Phys. **137**, 194504 (2012).
[14] P. Geiger and C. Dellago, J. Chem. Phys. **139**, 164105 (2013).
[15] S. Pipolo, M. Salanne, G. Ferlat, S. Klotz, A. M. Saitta, and F. Pietrucci, Phys. Rev. Lett. **119**, 245701 (2017).
[16] S. Prestipino, J. Chem. Phys. **148**, 124505 (2018).
[17] T. Li, D. Donadio, G. Russo, and G. Galli, Phys. Chem. Chem. Phys. **13**, 19807 (2011).
[18] T. Li, D. Donadio, and G. Galli, Nat. Commun. **4**, 1887 (2013).
[19] A. Haji-Akbari and P. G. Debenedetti, Proc. Natl. Acad. Sci. U.S.A. **112**, 10582 (2015).
[20] A. Laio and M. Parrinello, Proc. Natl. Acad. Sci. U.S.A. **99**, 12562 (2002).
[21] A. Barducci, G. Bussi, and M. Parrinello, Phys. Rev. Lett. **100**, 020603 (2008).
[22] A. Laio and F. L. Gervasio, Rep. Prog. Phys. **71**, 126601 (2008).
[23] Y. I. Yang, H. Niu, and M. Parrinello, J. Phys. Chem. Lett. **9**, 6426 (2018).
[24] G. M. Torrie and J. P. Valleau, J. Comput. Phys. **23**, 187 (1977).
[25] O. Valsson and M. Parrinello, Phys. Rev. Lett. **113**, 090601 (2014).
[26] H. Niu, P. M. Piaggi, M. Invernizzi, and M. Parrinello, Proc. Natl. Acad. Sci. U.S.A. **115**, 5348 (2018).
[27] M. S. Shell, P. G. Debenedetti, and A. Z. Panagiotopoulos, Phys. Rev. E **66**, 011202 (2002).
[28] J. Abascal, E. Sanz, R. García Fernández, and C. Vega, J. Chem. Phys. **122**, 234511 (2005).
[29] B. J. Murray, D. A. Knopf, and A. K. Bertram, Nature (London) **434**, 202 (2005).
[30] T. L. Malkin, B. J. Murray, A. V. Brukhno, J. Anwar, and C. G. Salzmann, Proc. Natl. Acad. Sci. U.S.A. **109**, 1041 (2012).
[31] E. B. Moore and V. Molinero, Phys. Chem. Chem. Phys. **13**, 20008 (2011).
[32] See Supplemental Material at http://link.aps.org/supplemental/10.1103/PhysRevLett.122.245501 for details about the computational setup and other materials, which also includes Refs. [33–36].
[33] G. A. Tribello, M. Bonomi, D. Branduardi, C. Camilloni, and G. Bussi, Comput. Phys. Commun. **185**, 604 (2014).
[34] G. Bussi, D. Donadio, and M. Parrinello, J. Chem. Phys. **126**, 014101 (2007).
[35] T. Wieder, J. Math. Comput. Sci. **2**, 1086 (2012).
[36] E. Giuffré, S. Prestipino, F. Saija, A. M. Saitta, and P. V. Giaquinta, J. Chem. Theory Comput. **6**, 625 (2010).
[37] P. M. Piaggi, O. Valsson, and M. Parrinello, Phys. Rev. Lett. **119**, 015701 (2017).
[38] P. M. Piaggi and M. Parrinello, Proc. Natl. Acad. Sci. U.S.A. **115**, 10251 (2018).
[39] M. Conde, M. Rovere, and P. Gallo, J. Chem. Phys. **147**, 244506 (2017).
[40] M. Parrinello and A. Rahman, J. Appl. Phys. **52**, 7182 (1981).
[41] T. L. Malkin, B. J. Murray, C. G. Salzmann, V. Molinero, S. J. Pickering, and T. F. Whale, Phys. Chem. Chem. Phys. **17**, 60 (2015).
[42] L. Bonati and M. Parrinello, Phys. Rev. Lett. **121**, 265701 (2018).
[43] B. J. Murray, C. G. Salzmann, A. J. Heymsfield, S. Dobbie, R. R. Neely, III, and C. J. Cox, Bull. Am. Meteorol. Soc. **96**, 1519 (2015).
[44] S. Auer and D. Frenkel, J. Chem. Phys. **120**, 3015 (2004).
[45] S. Auer and D. Frenkel, Nature (London) **409**, 1020 (2001).
[46] J. Espinosa, E. Sanz, C. Valeriani, and C. Vega, J. Chem. Phys. **141**, 18C529 (2014).
[47] J. Espinosa, C. Navarro, E. Sanz, C. Valeriani, and C. Vega, J. Chem. Phys. **145**, 211922 (2016).

[48] H. Pruppacher, J. Atmos. Sci. **52**, 1924 (1995).
[49] B. Murray, S. Broadley, T. Wilson, S. Bull, R. Wills, H. Christenson, and E. Murray, Phys. Chem. Chem. Phys. **12**, 10380 (2010).
[50] B. Riechers, F. Wittbracht, A. Hütten, and T. Koop, Phys. Chem. Chem. Phys. **15**, 5873 (2013).
[51] P. Stöckel, I. M. Weidinger, H. Baumgärtel, and T. Leisner, J. Phys. Chem. A **109**, 2540 (2005).
[52] B. Murray, D. O'sullivan, J. Atkinson, and M. Webb, Chem. Soc. Rev. **41**, 6519 (2012).
[53] B. Krämer, O. Hübner, H. Vortisch, L. Wöste, T. Leisner, M. Schwell, E. Rühl, and H. Baumgärtel, J. Chem. Phys. **111**, 6521 (1999).
[54] W. Cantrell and A. Heymsfield, Bull. Am. Meteorol. Soc. **86**, 795 (2005).
[55] D. Rzesanke, J. Nadolny, D. Duft, R. Müller, A. Kiselev, and T. Leisner, Phys. Chem. Chem. Phys. **14**, 9359 (2012).
[56] S. Benz, K. Megahed, O. Möhler, H. Saathoff, R. Wagner, and U. Schurath, J. Photochem. Photobiol. A **176**, 208 (2005).
[57] H. Laksmono, T. A. McQueen, J. A. Sellberg, N. D. Loh, C. Huang, D. Schlesinger, R. G. Sierra, C. Y. Hampton, D. Nordlund, M. Beye *et al.*, J. Phys. Chem. Lett. **6**, 2826 (2015).
[58] D. E. Hagen, R. J. Anderson, and J. L. Kassner, Jr., J. Atmos. Sci. **38**, 1236 (1981).
[59] A. J. Amaya and B. E. Wyslouzil, J. Chem. Phys. **148**, 084501 (2018).
[60] Y. Xu, N. G. Petrik, R. S. Smith, B. D. Kay, and G. A. Kimmel, J. Phys. Chem. Lett. **8**, 5736 (2017).
[61] J. R. Espinosa, C. Vega, and E. Sanz, J. Phys. Chem. C **122**, 22892 (2018).
[62] J. A. Sellberg, C. Huang, T. A. McQueen, N. Loh, H. Laksmono, D. Schlesinger, R. Sierra, D. Nordlund, C. Hampton, D. Starodub *et al.*, Nature (London) **510**, 381 (2014).
[63] H. Tanaka, Eur. Phys. J. E **35**, 113 (2012).
[64] E. B. Moore and V. Molinero, Nature (London) **479**, 506 (2011).
[65] G. Bullock and V. Molinero, Faraday Discuss. **167**, 371 (2013).
[66] M. Fitzner, G. C. Sosso, S. J. Cox, and A. Michaelides, Proc. Natl. Acad. Sci. U.S.A. **116**, 2009 (2019).
[67] J. R. Errington, P. G. Debenedetti, and S. Torquato, Phys. Rev. Lett. **89**, 215503 (2002).
[68] J. Russo, F. Romano, and H. Tanaka, Nat. Mater. **13**, 733 (2014).
[69] S. Overduin and G. Patey, J. Chem. Phys. **143**, 094504 (2015).
[70] P. Pirzadeh, E. N. Beaudoin, and P. G. Kusalik, Chem. Phys. Lett. **517**, 117 (2011).
[71] P.-L. Chau and A. Hardwick, Mol. Phys. **93**, 511 (1998).
[72] J. R. Errington and P. G. Debenedetti, Nature (London) **409**, 318 (2001).